AN INTEGRATED ULTRASOUND TRANSDUCER DRIVER FOR HIFU APPLICATIONS

Wai Wong, Carlos Christoffersen, Samuel Pichardo, Laura Curiel

Lakehead University, Thunder Bay, ON, P7B 5E1
Department of Electrical and Computer Engineering
Email: wlwong1, carlos.christoffersen, spichard, lcuriel@lakeheadu.ca

ABSTRACT

This paper presents for the first time an MRI-compatible integrated CMOS amplifier capable of directly driving a piezoelectric ultrasound transducer for High Intensity Focused Ultrasound (HIFU) applications. The amplifier operates in class DE mode loaded with a piezoelectric ultrasound transducer connected in parallel with a shunt capacitor. There is no need for external inductors. The integrated amplifier is implemented with the Teledyne-DALSA 0.8 μm CMOS process. Modeling of the piezoelectric transducer and amplifier design considerations are presented, followed by simulation results obtained using the Spectre simulator. The proposed design achieves over 80% efficiency with 1 W of output power at 1 MHz and an acceptable third harmonic level. The estimated die area of the amplifier is 2 mm^2.

Index Terms— piezoelectric transducer driver, ultrasound transducer, HIFU, class DE amplifier

1. INTRODUCTION

HIFU, or High Intensity Focused Ultrasound, is a non-invasive surgical technique that thermally ablates tissue in human organs without the need of incision. Tumor ablation is achieved by focusing acoustic energy that translates into heat energy delivered to the focal zone of the ultrasound transducer [1]. As it is a very precise operation, any movements of the patient's body may displace the focal zone; in other words, good tissue may be damaged. HIFU operation can be guided by Magnetic Resonance Imaging (MRI) such that any body movements can be compensated in real time. These developments require the use of multi-element ultrasonic transducers. This allows controlling the location where the energy is focused by electronically driving each element at a different phase. The advantage of this approach is that we can dynamically reach different locations. Using multiple independent elements increase the complexity of the connections and driving electronics required to pilot HIFU devices. There is considerable interest both at the research and commercial levels for developing new and improved electronic systems for HIFU that can drive multi-element devices with as many as 1000 elements at an affordable cost. By providing a driving system that can pilot a large number of elements with enough power to achieve therapeutic levels, we could achieve the necessary degree of freedom to concentrate the HIFU energy where it is needed. Furthermore, this system should allow piloting devices that are under MRI guidance, providing thermal control for the therapy. This work reports progress towards that goal.

We propose an MRI-compatible, integrated CMOS class DE amplifier that can directly drive a piezoelectric ultrasound transducer with high efficiency and reasonable harmonic distortion. One of the challenges of developing an MRI-compatible device is to eliminate the use of magnetic components, such as inductors. Most high power drivers for piezoelectric ultrasound transducers require external matching networks or external inductors that would be too large for a compact system and likely interfere with the MRI-guidance system. Hall and Cain [2] proposed a low-cost high-efficiency amplifier for driving transducer arrays; however, the proposed design requires an LC circuit to attenuate harmonics from the output. Inductors can change the behavior of a capacitive load to inductive, and be used as a harmonic content filter, but ferrite core inductors are incompatible with the MRI environment. In addition, exciting a piezoelectric transducer with square wave will cause the transducer to produce unwanted sidelobes in the acoustic power field. [3] These sidelobes will eventually distort the shape of the focal zone and the precision of the focusing point. Tang and Clement [3] evaluated the performance of the harmonic cancellation technique for a therapeutic ultrasound transducer in HIFU applications. However, the proposed amplifier requires a transformer that cannot be integrated on-chip. Lewis and Olbricht [4] developed a high-efficiency amplifier for a high intensity ultrasound system without using an external matching circuit, but exciting an ultrasound transducer with a square wave is not suitable for HIFU applications and the design is not small enough for a compact solution. Ang *et al.* [5] have fabricated an integrated amplifier chip for ultrasound dental tissue healing. Although it has a power efficiency of 70% and an output power of 0.58 W, it requires an external LC matching network.

The remainder of this paper is organized as follows:

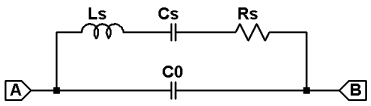

Fig. 1. Butterworth Van Dyke (BVD) equivalent circuit. C_0 is the static capacitor of the PZT crystal. R_s, L_s, and C_s describe the mechanical oscillator at its resonant frequency.

Section 2 describes the transducer characterization and Section 3 discusses the proposed design, output stage, MOSFET gate driver and simulation results.

2. TRANSDUCER CHARACTERIZATION

A piezoelectric resonator has multiple resonant frequencies. The impedance characteristics of a piezoelectric resonator close to one of its resonant frequencies can be represented by the Butterworth Van Dyke (BVD) equivalent circuit as shown in Figure 1, [6]. The complex impedance of a BVD equivalent circuit near its resonant frequency can be expressed as

$$Z = \frac{\frac{1}{j\omega C_0}\left(\frac{1}{j\omega L_S} + R_S + j\omega L_S\right)}{\frac{1}{j\omega C_0} + \frac{1}{j\omega L_S} + R_S + j\omega L_S} \tag{1}$$

At resonant frequency ω_s, the complex impedance Z_s is

$$Z_s|_{\omega=\omega_s} = \frac{\frac{R_s}{j\omega_s C_0}}{\frac{1}{j\omega_s C_0} + R_s} \tag{2}$$

We solve for C_0 and R_s:

$$C_0 = \frac{-Im(Z_s)}{2\pi f_s |Z_s|^2} \tag{3}$$

$$R_S = \frac{|Z_s|^2}{Re(Z_s)} \tag{4}$$

Equations for C_s and L_s are available in [6]:

$$C_s = C_0\left[\left(\frac{f_p}{f_s}\right)^2 - 1\right] \tag{5}$$

$$L_s = \frac{1}{(2\pi f_s)^2 C_s} \tag{6}$$

where f_s represents the series resonant frequency, and the imaginary component of the series resonant branch equals zero; f_p is the parallel resonant frequency where the real component of the impedance is maximum. Equations (3) to (6) are applied at each resonant frequency to calculate the LRC values of independent branches. The transducer model is formed by connecting all branches in parallel.

The impedance of a piezoelectric crystal had been measured using a Vector Network Analyzer (VNA). A

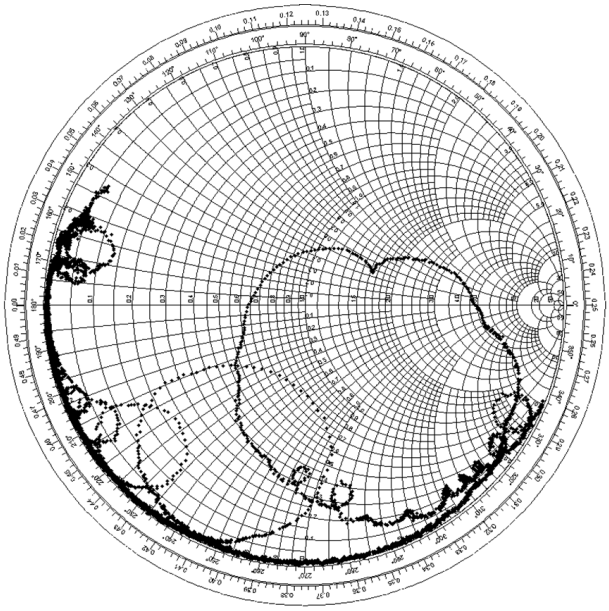

Fig. 2. The impedance of the crystal from 300 kHz to 300 MHz

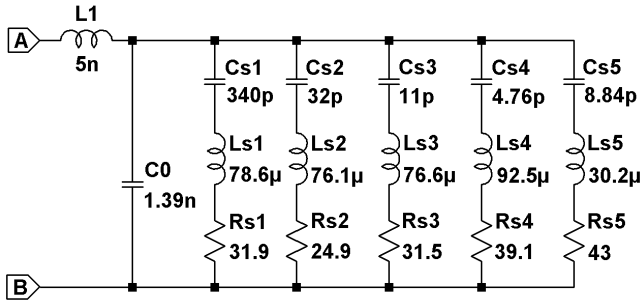

Fig. 3. Equivalent circuit for the crystal. It behaves inductively at high frequency mainly due to the fact that three short conducting wires are used to connect to the amplifier.

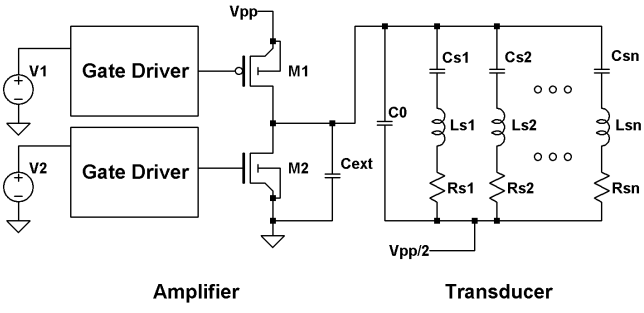

Fig. 4. Simplified schematic diagram of the proposed integrated amplifier. The output stage employs a single shunt class DE amplifier and its output network is replaced by an ultrasound transducer.

calibration procedure was followed to remove the effects of cables and connectors. Figure 2 shows the impedance characteristics of the piezoelectric crystal on a Smith chart. Each of the several resonance loops observed in that figure is modeled with an independent RLC branch in the equivalent circuit model. Figure 3 shows the equivalent circuit of the crystal.

3. PROPOSED DESIGN

The proposed integrated driver will attach at the back of a 25 mm diameter, 50 mm curvature PZT piezoelectric crystal. The driver has an output power of 1 W at 1 MHz and an estimated die area of approximately 2 mm^2. As shown in Figure 4, the output of the amplifier connects to a piezoelectric crystal directly. The amplifier and gate driver are implemented with a class DE amplifier and a static level shifter respectively.

3.1. Output Stage

A class DE amplifier uses the same topology as the class D amplifier but operates at Class E switching conditions because of its output network. The output network of the class DE amplifier is composed by the ultrasound transducer in parallel with a capacitor (C_{ext}) as shown in Figure 4. The major advantages of using a class DE amplifier is that its theoretical efficiency can be as high as 100% and that no external inductors are required. The ideal operation of a class DE amplifier is described in detail in [7] and [8]. Since the part of the output network is fixed by the equivalent circuit of the transducer, the amplifier will operate in non-optimum condition [9]. The shunt capacitor can be calculated as shown below [7]:

$$C_{shunt} = \frac{1}{\pi \omega_s R_{s1}} \tag{7}$$

where ω_s is the series resonant frequency of the fundamental branch, and R_{s1} is the resistor of the fundamental branch. In this case, the external capacitor C_{ext} is given by:

$$C_{ext} = C_{shunt} - C_0 - 2C_{drain} \tag{8}$$

where C_0 is the transducer′s static capacitor; C_{drain} is the drain capacitance of the power MOSFET M1 and M2. Since the output network is fixed by the equivalent circuit of the transducer, the amplifier will operate in non-optimum condition [9] and the calculated value of C_{ext} has to be readjusted to account for this condition.

Both M1 and M2 are high voltage transistors that can withstand a drain to source voltage of 20 V. They will occupy an estimated area of 0.7 mm^2. Each power transistor is assembled from 100 transistors with a width of $100\,\mu m$ and they are connected in parallel to establish a low output impedance.

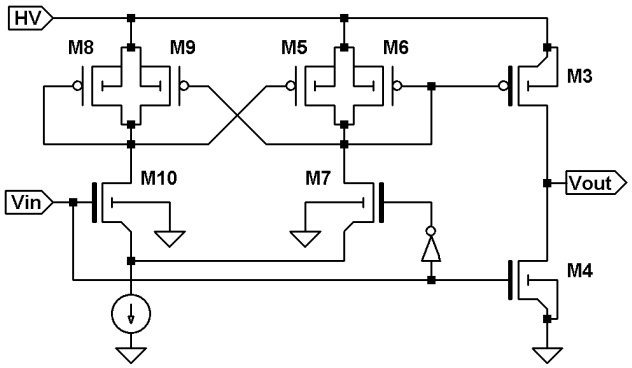

Fig. 5. Static level shifter as power MOSFETs gate driver

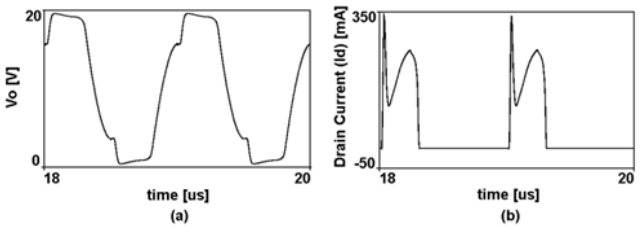

Fig. 6. a) Steady state output voltage b) Steady state drain current of PMOS transistor M1.

3.2. Gate Driver

A static level shifter (Figure 5) [10], converts a 5 V logic signal to a 20 V gate signal for the amplifier stage. It offers high speed switching without the need for multiple driving signals. However, the major disadvantage of a static level shifter is constant power consumption. Therefore, current flow through voltage mirrors, M5, M6 and M8, M9 must be analyzed carefully to compromise between power consumption and performance. In Figure 5, M5, M6, M8 and M9 are standard 5 V PMOS; M4, M7 and M10 are high-voltage NMOS and M3 is a high-voltage PMOS.

Another functionality of the level shifter is to control the rise and fall time of the gate driving signals that feed into the class DE stage. The channel resistance of M3 and M4 and the input capacitance of M1 or M2 determine the rise time and fall time of the gate signals. The 10 to 90% rise time or fall time is approximated by

$$t = 2.2 R_{ch} C_{total} \tag{9}$$

where R_{ch} is the channel resistance of M3 or M4 and C_{total} is the total load capacitance.

$$C_{total} = C_{in,\,M1} + C_{drain,\,M3} + C_{drain,\,M4} \tag{10}$$

Table 1. Comparison of specifications of the proposed design and other published works

References	Frequency	Efficiency	Output Power	Implementation	Output Matching	Excitation
[2]	1 MHz		20 W	discrete components	LC network	sine wave
[3]	1 MHz			discrete components	transformer	sine wave
[4]	1 to 10 MHz	90%	50 W	discrete components	none	square wave
[5]	1.5 MHz	70%	0.58 W	integrated circuit	LC network	sine wave
Proposed design	1 MHz	80%	1 W	integrated circuit	shunt capacitor	class DE waveform

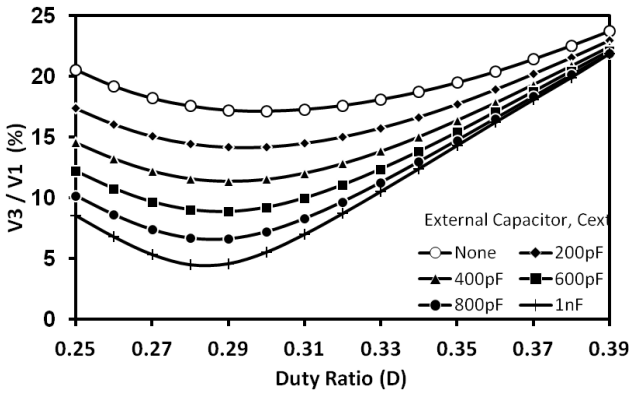

Fig. 7. Ratio of third harmonic to fundamental from the output waveform as a function of duty ratio with various external capacitances at steady state. D represents switch-on ratio of each MOSFET per period of time including turn-on and turn-off delays.

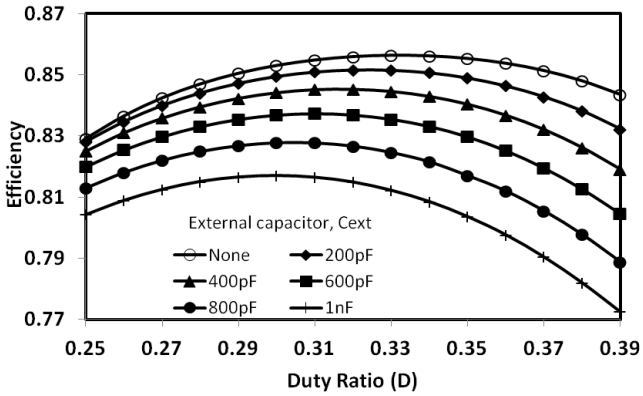

Fig. 8. Steady state efficiency as a function of duty ratio

3.3. Simulation Results

All simulations were performed using the Spectre® simulator. Since the output stage directly connects to an ultrasound transducer instead of through a tuned network, the class DE amplifier is not operating at its optimum working condition and this is shown in Figure 6a. Optimization of C_{ext} and the switch-on duty ratio (D) was performed to improve efficiency and reduce third harmonic. Figure 6b shows the corresponding drain current of PMOS transistor M1. The initial current peaks produce switching losses and should be minimized.

Increasing the external capacitance of the class DE

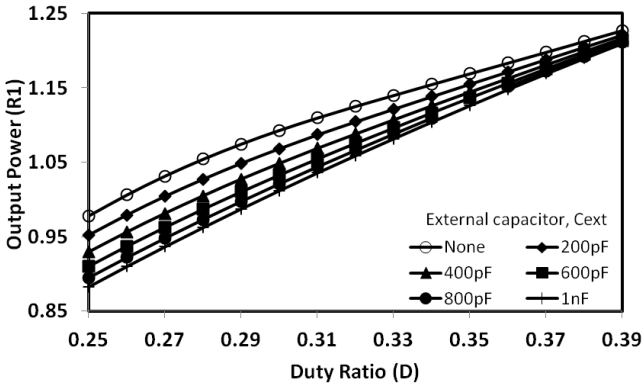

Fig. 9. Steady state output power as a function of duty ratio

amplifier reduces the third harmonic in the output voltage waveform; however, it increases the peak of drain current spike because of the increased capacitive load. Figure 7 shows that the third harmonic becomes lowest when the duty ratio D is between 0.28 to 0.3 at steady state. The third harmonic was approximately 18% of the fundamental without any additional external capacitor and below 5% with an external capacitor of 1 nF. Figure 8 is the summary of drivers efficiency as a function of duty ratio. As the external capacitance increases, the driver efficiency decreases and the gaps between curves become wider; however, the efficiency of the amplifier is still higher than 80% in general. Finally, Figure 9 is another summary of output power to R_{s1} with various parameters. The initial recommended duty ratio of the integrated amplifier is 0.28 without shunt capacitor. Because of the turn-on and turn-off delays from the power MOSFET, the duty ratio of the control signal should be 0.22. The proposed amplifier will operate at non-optimum class DE condition and it has an output power of 1.08 W and an efficiency of 84%.

4. CONCLUSION

This work presents the design of the first MRI-compatible integrated amplifier for driving an ultrasonic therapeutic piezoelectric transducer in HIFU applications. Using a class DE amplifier as the output stage, the need for an external inductor between the amplifier and the piezoelectric crystal can be eliminated. Increasing the capacitance of the external capacitor reduces the third harmonic; however, this also reduces the amplifiers efficiency as a trade off. It is important to note that the acoustic third harmonic is expected to be lower than the electrical third harmonic shown in this paper. A comparison of other published works with the proposed design can be found in Table 1. Several steps remain to be performed in order to produce a practical compact multi-element HIFU driver. The next planned step is to fabricate and test the proposed amplifier.

5. ACKNOWLEDGEMENTS

The authors would like to thank the National Research Council of Canada (NSERC) and CMC Microsystems for supporting this work.

6. REFERENCES

[1] G. Ter Haar, "Ultrasound focal beam surgery," *Ultrasound in Medicine and Biology*, vol. 21, no. 9, pp. 1089–1100, 1995.

[2] T. Hall and C. Cain, "A low cost compact 512 channel therapeutic ultrasound system for transcutaneous ultrasound surgery," *AIP Conference Proceedings*, vol. 829, no. 1, pp. 445–449, May 8 2006.

[3] S. C. Tang and G. T. Clement, "A harmonic cancellation technique for an ultrasound transducer excited by a switched-mode power converter," in *Proc. IEEE Ultrasonics Symp.*, 2008, pp. 2076–2079.

[4] G. Lewis and W. Olbricht, "Design and characterization of a high-power ultrasound driver with ultralow-output impedance," *Review of Scientific Instruments*, vol. 80, no. 11, pp. 114704, 2009.

[5] W. T. Ang, C. Scurtescu, W. Hoy, T. El-Bialy, Y. Y. Tsui, and J. Chen, "Design and implementation of therapeutic ultrasound generating circuit for dental tissue formation and tooth-root healing," *IEEE Trans. on Biomedical Circuits and Systems*, vol. 4, no. 1, pp. 49–61, 2010.

[6] "IEEE Standard Definitions and Methods of Measurement for Piezoelectric Vibrators," 1966.

[7] M. Kazimierczuk, *RF Power Amplifiers*, chapter Class DE RF Power Amplifier, pp. 251–266, Wiley, Chichester, West Sussex, U.K., 2008.

[8] M. Albulet, "An exact analysis of Class-DE amplifier at any output Q," *IEEE Trans. Circuits and Systems I*, vol. 46, no. 10, pp. 1228–1239, Oct 1999.

[9] H. Sekiya, T. Negishi, T. Suetsugu, and T. Yahagi, "Operation of Class DE amplifier outside optimum condition," in *Proc. of IEEE International Symposium on Circuits and Systems (ISCAS 2006)*, May 2006, p. 4.

[10] H. Ballan and M. Declercq, *High Voltage Devices and Circuits in Standard CMOS Technologies*, chapter High-Voltage Analog and Digital Output Interfaces, pp. 181–207, Kluwer Academic Publishers, Dordrecht, Netherlands, 1999.